Evidence for product specific active sites on oxide-derived Cu catalysts for electrochemical CO_2 reduction

Yanwei Lum[1,2] and Joel W. Ager[1,2,*]

[1]Joint Center for Artificial Photosynthesis and Materials Sciences Division, Lawrence Berkeley National Laboratory, California 94720, United States.
[2]Department of Materials Science and Engineering, University of California, Berkeley, California 94720, United States

*Email: jwager@lbl.gov (J.W.A.)

CO_2 electroreduction in aqueous media using Cu catalysts can generate many different C_2/C_3 products, leading to the question whether all products are generated from the same types of active sites or if product specific active sites are responsible for making certain products. Here, by reducing mixtures of ^{13}CO and $^{12}CO_2$, we show that oxide derived (OD) Cu catalysts have 3 different types of active sites for C-C coupled products, one for producing ethanol/acetate, another for ethylene and yet another for 1-propanol. In contrast, we do not find evidence of product specific sites on polycrystalline Cu and oriented (100) and (111). Analysis of the isotopic composition of the products leads to the prediction that the adsorption energy of *COOH (product of the first step of CO_2 reduction) may be a descriptor for the product selectivity of a given active site. These new insights should enable highly selective catalysts to be developed.

The last few decades alone have seen large increases in atmospheric CO_2 concentrations, mainly due to mankind's consumption of fossil fuels for energy.[1] It has been projected that global energy consumption will continue to rise, leading to tripling of CO_2 emissions by 2040.[1] There is therefore an urgent need to develop technologies capable of efficiently harvesting and storing renewable energy to reduce our dependence on fossil fuels.[2]

Electrochemical CO_2 reduction (CO_2R) in aqueous media presents an attractive and viable strategy to reduce carbon emissions by directly converting CO_2 into valuable hydrocarbons and oxygenates such as ethylene and ethanol.[3,4] To date, Cu remains the most promising catalyst capable of driving this conversion process at reasonable current densities.[5,6] While methane, ethylene, and ethanol are the major products, up to 18 different possible products can be produced.[7–9] It is commonly accepted that except for formate, CO_2R on Cu is initiated by reducing CO_2 to adsorbed CO (*CO).[10–13] Further protonation of *CO results in methane/methanol formation (C_1 pathway) or *CO can couple with another *CO (C-C coupling), leading to C_2/C_3 products such as ethylene and 1-propanol.[14–16] However, although there have been intriguing reports of selective ethylene production under a certain range of conditions and at high current densities[17,18], it has been experimentally difficult to control selectivity to a given C_2 or C_3 product. To further improve catalyst performance and selectivity, it is crucial to first identify and understand the nature of the active sites that are present on Cu electrocatalysts. A related and important question is whether all products are produced from the same active sites or if specific active sites are responsible for generating a given product. In other words, are there product specific active sites that mostly generate only one product?

We reasoned that it would be possible to answer these critical questions by performing electroreduction of a mixture of ^{13}CO and $^{12}CO_2$. To explain our rationale, consider a hypothetical catalyst that possesses only 2 types of active sites for C_2 production (see Fig. 1). We assume that one site (A) is selective for ethylene while the other (B) is selective for ethanol.

Because their catalytic properties are different, we would expect that the adsorption energies of intermediates, often used as a descriptor for catalytic activity,[19–21] should also be different on the two sites. Due to the difference in intermediate adsorption energies, we would naturally expect that the turn over frequencies for generating these intermediates will be different. As a specific example, the rate of the initial step of CO_2R, converting CO_2 to *CO, will be different on the two sites. As a result, if we were to reduce a mixture of ^{13}CO and $^{12}CO_2$, the turn over frequency for $^{12}CO_2$ reduction to $*^{12}CO$ should be active site dependent, resulting in sites A and B having different probabilities of being occupied by $*^{12}CO$ vs $*^{13}CO$. In this case, we assume that the turn over frequency of $^{12}CO_2$ reduction to $*^{12}CO$ is higher for site B, leading to a higher (lower) probability of $*^{12}CO$ ($*^{13}CO$) on this site.

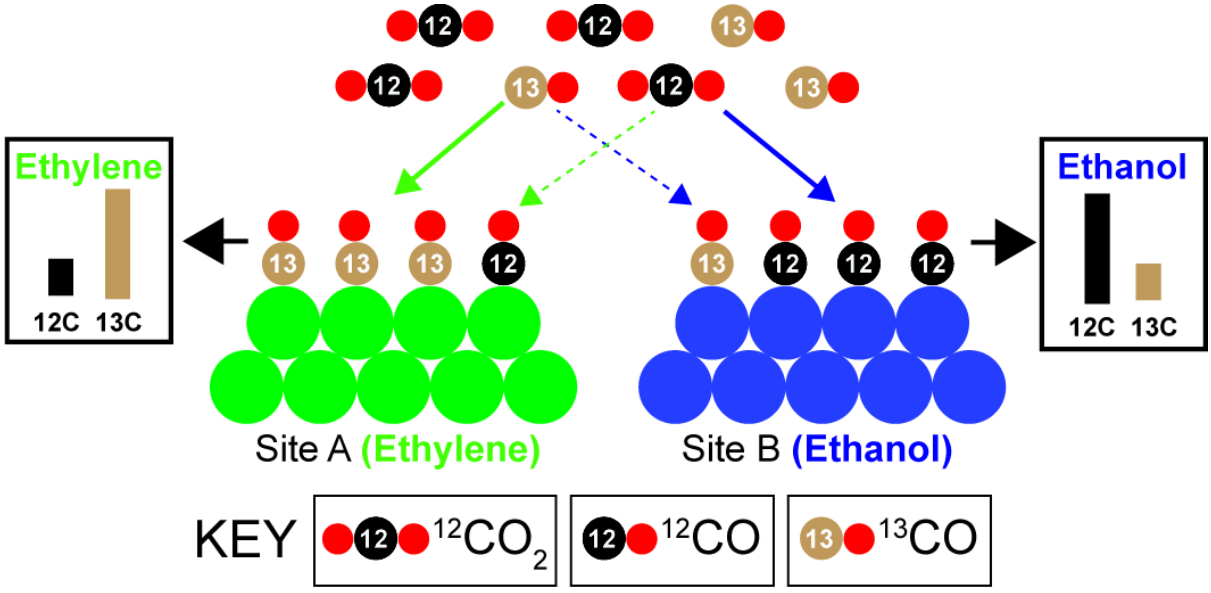

Fig. 1 | Hypothetical scenario in which reduction of a mixture of ^{13}CO and $^{12}CO_2$ is carried out on a catalyst with 2 types of active sites, A and B. Site A favours ethylene formation (green) while site B favours ethanol formation (blue). Also, it is assumed that the turn over frequency of $^{12}CO_2$ reduction to $*^{12}CO$ is higher for ethanol selective sites, leading to a higher probability of $*^{12}CO$ on site B. This results in ethylene having more ^{13}C compared to ethanol.

In the next electrocatalytic step, C-C coupling between the *CO on the sites, followed by a series of proton-coupled electron transfers and dehydration steps[16,22–24], results in formation of ethylene (for site A) and ethanol (for site B). Crucially, the isotopic composition of the products will be different: in this hypothetical case, ethylene will have more ^{13}C than

ethanol. More generally, this analysis shows that if a mixture of ^{13}CO and $^{12}CO_2$ is reduced, the isotopic composition of the C-C coupled products will serve as a fingerprint of the active sites which produced them. That is, if two C-C coupled products have different isotopic compositions, then they have been produced by different types of active sites. On the other hand, if the catalyst does not have product specific active sites, then all products should have similar isotopic compositions.

In this work, we apply this isotope labelling concept to analyse the active sites on oxide-derived (OD) Cu catalysts. Such catalysts are typically prepared by oxidation of a Cu foil/film, followed by reduction to its metallic state.[25–29] This class of catalysts, originally reported by Kanan and co-workers, is of significant interest because they have shown dramatically reduced overpotentials for the reduction of CO to oxygenate products (e.g. ethanol) with high faradaic efficiencies.[27,30] Furthermore, work from many research groups have shown that these catalysts exhibit enhanced selectivity for reducing CO_2 to C_2/C_3 products, whilst suppressing the formation of C_1 products.[25,26,28,31–33]

There have been a number of studies aimed at identifying the active sites responsible for the unique catalytic properties of OD Cu. Chorkendorff and co-workers used temperature programmed desorption to detect strong CO binding sites that are not present on polycrystalline Cu.[34] They posited that these strong binding sites could be the grain boundaries observed in their OD Cu catalysts. In related work, Kanan and co-workers demonstrated that grain boundaries are the active sites for reduction of CO to C_2/C_3 products.[34,35] However, it is not known whether all the grain boundaries are active or if only the ones with specific structures are responsible for generating most of the products.

The objective of this work is to determine if product specific active sites are responsible for the superior C_2/C_3 selectivity of OD Cu. Evidence of product specific sites will motivate future studies to understand how each of these different active sites work and to develop methods for building specific types of product specific sites into a single structure, both of which could lead to CO_2R catalysts with greatly improved product

selectivity. Indeed, we have discovered that OD Cu has at least three types of active sites which selectively produce ethylene, ethanol/acetate and 1-propanol, respectively. In contrast, polycrystalline Cu and as well as Cu (100) and Cu (111) oriented surfaces do not appear to have product specific active sites.

Results

Reduction of ^{13}CO and $^{12}CO_2$ mixtures. Due to the large differences in the aqueous solubility between ^{13}CO (1 mM) and $^{12}CO_2$ (33.4 mM), selecting their ratio to achieve a given ^{12}CO:^{13}CO surface coverage merits some discussion. Based on calculations and experiments (Supplementary Figs. 1-2), we estimated that a 70:30 ratio of ^{13}CO to $^{12}CO_2$ would allow for similar rates of $*^{13}CO$ and $*^{12}CO$ formation to occur. OD Cu catalysts were prepared according to procedures described by Kanan and co-workers[27] (Supplementary Figs. 3-5). Polycrystalline Cu (PC Cu) was prepared by electropolishing of Cu foil and oriented surfaces of Cu (100) and Cu (111) were fabricated using procedures developed by Jaramillo and co-workers.[36] Natural abundance CO_2 reduction in 0.1 M $KHCO_3$ with these catalysts qualitatively reproduced previously reported results (Supplementary Fig. 6 and Supplementary Figs. 8-10). Natural abundance CO reduction in 0.1 M KOH (Supplementary Fig. 7) confirmed that our OD Cu catalysts performed similarly to those reported by Kanan and co-workers.[27] Gas chromatography-mass spectrometry (GCMS) and ^{13}C NMR were employed to determine the isotopic composition of the gas and liquid products (see Methods and Supplementary Figs. 11-23 and Supplementary Tables 1-8 for details). For experimental validation we reduced $^{13}CO/^{12}CO$ in ratios of 1:3, 1:1 and 3:1 on the OD Cu catalyst and observed the expected statistical isotope compositions and distributions (see Supplementary Tables 9-14 for details). Throughout this work, we will refer to the isotopic composition as the fraction of ^{13}C in the product. Additionally, the ^{12}C-^{13}C distribution, for example of ethylene, refers to the fractions of the 3 possible product variants: $^{12}CH_2{}^{12}CH_2$, $^{12}CH_2{}^{13}CH_2$ and $^{13}CH_2{}^{13}CH_2$.

Confident of our experimental and analytical methods, we proceeded to carry out the reduction of the 70:30 $^{13}CO/^{12}CO_2$ gas mixture with the oxide-derived Cu catalyst. Fig. 2a shows the isotopic compositions of ethylene, ethanol, acetate and 1-propanol produced by OD Cu at 4 different applied potentials in 0.1 M $KHCO_3$ electrolyte. There are a number of striking findings. Firstly, regardless of the applied potential, the isotopic composition (^{13}C fraction) of ethanol and acetate are identical, which strongly suggests that these products are generated from the same active sites. Secondly, it also appears that ethylene is produced from a different set of active sites, as evidenced by its consistently higher ^{13}C fraction as compared to ethanol/acetate. It is also observed that the ^{13}C fraction of ethylene changes more strongly with potential compared to the other products. Finally, 1-propanol also has a ^{13}C fraction that appears distinct from either that of ethylene or ethanol/acetate, which means that this product is generated by yet another set of active sites.

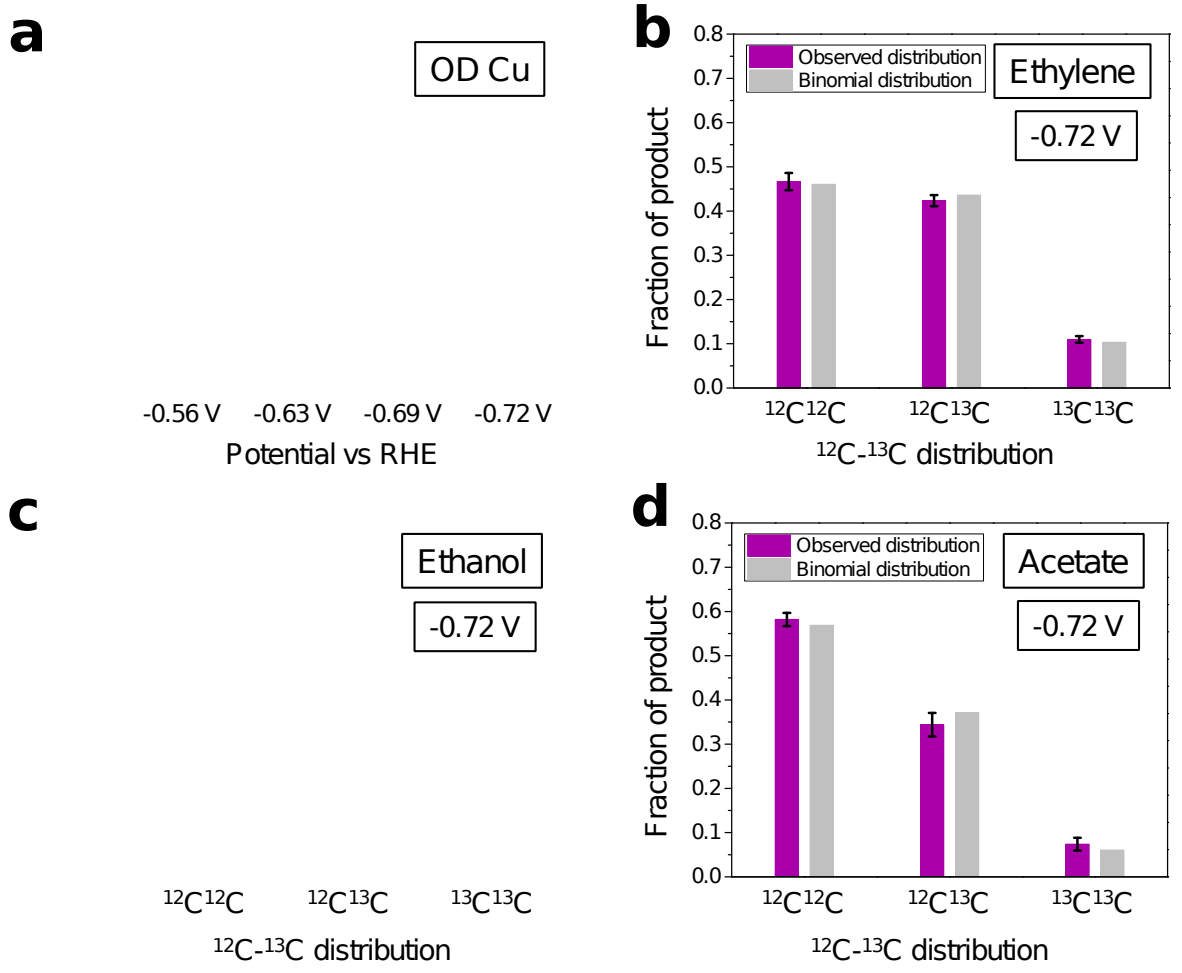

Fig. 2 | Isotopic compositions and ^{12}C-^{13}C distributions of products generated by OD Cu. (a) Isotopic composition (in terms of the ^{13}C fraction) of ethylene, ethanol, acetate and 1-propanol produced by reduction of the $^{13}CO/^{12}CO_2$ gas mixture with OD Cu at 4 different potentials. (b), (c) and (d) are ^{12}C-^{13}C distributions of ethylene, ethanol and acetate, respectively, at -0.72 V vs RHE. For the ^{12}C-^{13}C distributions at other potentials, see Supplementary Fig. 27. All distributions appear to be binomial, based on comparisons with the predicted binomial distribution based on the isotopic composition (calculation details in Supplementary Tables 3-5). Faradaic efficiency and current density data are shown in Supplementary Fig. 24. Catalyst stability data are shown in Supplementary Figs. 25-26. Error bars correspond to the standard deviation of 3 independent measurements.

A more detailed analysis of the isotopic compositions provides information on the properties of the different active sites. For these 4 products, it appears that the ^{13}C fraction decreases with more negative applied overpotential. This is likely due to the fact that at more negative applied overpotentials, the turn over frequency for converting $^{12}CO_2$ to $*^{12}CO$ on all active sites should increase, thereby increasing the probability of having a $*^{12}CO$ vs $*^{13}CO$ on all active sites. Since the ^{13}C fraction of ethanol/acetate is consistently lower than that of the other

products, it must mean that the active sites that generate these products have a higher probability of having a $*^{12}CO$. Therefore, the active sites that generate ethanol/acetate should have catalytic properties such that they are also able to drive $^{12}CO_2$ to $*^{12}CO$ with a turnover frequency larger than that of the ethylene active sites or 1-propanol active sites. Finally, the stronger potential dependence of the ^{13}C fraction of ethylene implies that the turn over frequency of $^{12}CO_2$ to $*^{12}CO$ should also have the largest potential dependence compared to the other active sites.

The notion that ethylene and ethanol/acetate are formed on product specific active sites on OD Cu is further supported by the binomial nature of their ^{12}C-^{13}C distributions. The ^{12}C-^{13}C distributions for these products at -0.72 V are shown in Figs. 2b-2d (see Supplementary Fig. 27 for the ^{12}C-^{13}C distributions at other potentials). As a comparison, the predicted binomial distributions for each product are shown as well in each of the figures (calculated based on the isotopic composition, see Supplementary Tables 3-5 for more details). If products were generated from multiple active sites which are not product specific, we would observe that the ^{12}C-^{13}C distribution would be a superposition of multiple binomial distributions, which would result in deviations from a true binomial distribution. Another observation is that the observed ^{12}C-^{13}C distributions of ethanol and acetate (Figs. 2c and 2d) appear to be identical, which is further evidence that these products are generated from the same active sites.

We have developed a multisite kinetic model which predicts product isotopic distributions as a function of the selectivity of the active sites, the $*^{13}CO$:$*^{12}CO$ ratio at a given site, and the number of active sites of a given type and their turnover frequency (see Supplementary Figs. 28-30 and Supplementary Table 15-17 for model details). The model allows consideration of effects which would cause the $*^{13}CO$:$*^{12}CO$ ratio to be similar for all sites such as surface diffusion of *CO and/or desorption and readsorption events. Clearly, the fact that we see differences in isotopic composition between the products means that reduction of CO to products necessarily outcompetes these isotopic scrambling effects. The model also shows that the sites must be substantially selective to observe

both differences in ^{13}C composition and a ^{12}C-^{13}C distribution which does not differ significantly from a binomial distribution.

Next, to determine if the existence of product specific active sites is a feature of Cu electrocatalysts in general, we performed reduction of the $^{13}CO/^{12}CO_2$ gas mixture with polycrystalline (PC) Cu, Cu (111) and Cu (100) oriented surfaces. Fig. 3a shows the isotopic composition of the products at -0.9 V vs RHE. In some cases, the isotopic compositions of acetate and 1-propanol could not be determined accurately as their formation rates were too low. In contrast to the case for OD Cu, we observe that the isotopic composition for the products generated are very similar, which means that these catalysts do not have product specific active sites. In Figs. 3b and 3c, the ^{12}C-^{13}C distributions of ethylene and ethanol generated by PC Cu appear to deviate slightly from the predicted binomial distribution. This might suggest that PC Cu may have multiple active sites which are not product specific. In this scenario, each type of active site might have a different probability of $*^{12}CO$ vs $*^{13}CO$, which results in the ^{12}C-^{13}C distributions of the products being a superposition of a few binomial distributions. To ensure that the similar isotopic compositions of the products was not just a coincidence, happening only at -0.9 V vs RHE, we tested Cu (100) at -0.8 V vs RHE. As expected, all products possess similar isotopic compositions, albeit with higher ^{13}C fractions due to the lower overpotential that was applied (Fig. 3d).

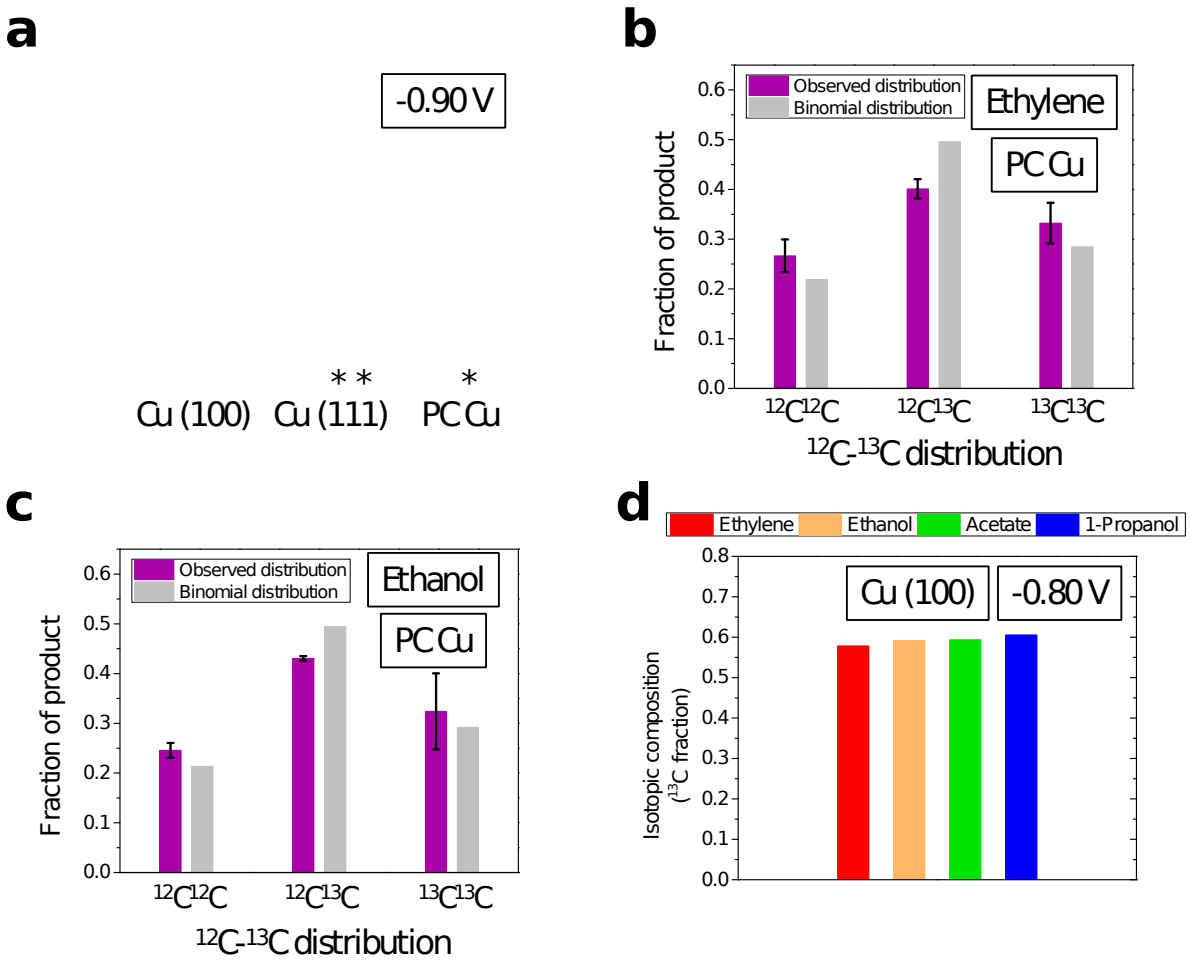

Fig. 3 | Isotopic compositions and ^{12}C-^{13}C distributions of products generated by Cu (111), Cu (100) and PC Cu. (a) Isotopic compositions (^{13}C fraction) of products generated by Cu (100), Cu (111) and PC Cu at -0.9 V vs RHE. The * in the figure appears whenever the isotopic composition could not be determined accurately. (b) and (c) Observed and predicted binomial ^{12}C-^{13}C distributions of ethylene and ethanol respectively for PC Cu. (d) Isotopic compositions (^{13}C fraction) of products generated by Cu (100) at -0.8 V vs RHE. ^{12}C-^{13}C distributions for Cu (100) and Cu (111) are shown in Supplementary Fig. 31. Catalysis data is shown in Supplementary Fig. 32. Error bars correspond to the standard deviation of 3 independent measurements.

Control experiments. We performed a series of control experiments to rule out local pH, surface area/roughness and catalyst morphology effects as possible explanations for our striking findings on OD Cu. Firstly, during CO_2R the local pH of the surface rises above the bulk pH because protons from water are consumed to drive reduction of CO_2 and hydrogen evolution.[3,37] This rise in local pH of the catalyst surface during CO_2R has been observed to suppress C_1 formation and enhance C-C coupling, thereby increasing selectivity towards C_2 products.[17,25,29,38] For high surface area catalysts such as OD Cu, the rise in local pH is larger as compared to

planar Cu electrodes due to the larger geometric current densities.[26] Therefore, to minimize local pH changes, we reduced the $^{13}CO/^{12}CO_2$ gas mixture with OD Cu in a 0.1 M phosphate buffer (pH 7.2) at a potential of -0.63 V. Such a buffer has been previously shown to be effective in significantly mitigating rises in local pH.[3,28,39] Fig. 4a shows that the isotopic compositions of ethylene, ethanol/acetate and 1-propanol remain distinct from each other in phosphate buffer, which allows us to rule out local pH effects as a possible explanation for our results.

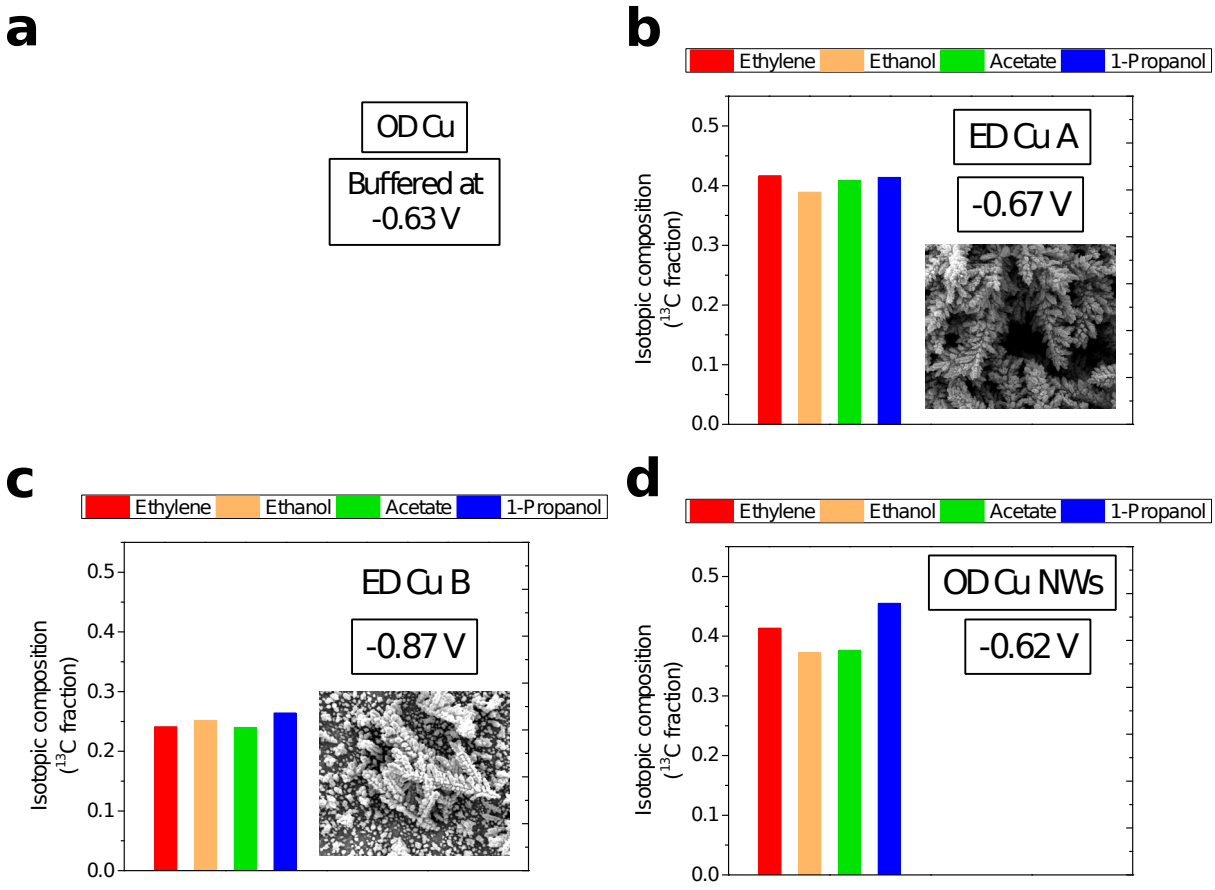

Fig. 4 | Isotopic compositions of products generated in control experiments. Isotopic compositions (^{13}C fraction) of products generated by (a) OD Cu in 0.1 M phosphate buffer at a potential of -0.63 V vs RHE, SEM image shown as inset with scale bar 1 µm. (b) ED Cu A at -0.67 V in 0.1 M $KHCO_3$, SEM image shown as inset with scale bar 4 µm. (c) ED Cu B at -0.87 V in 0.1 M $KHCO_3$, SEM image shown as inset with scale bar 4 µm. (d) OD Cu NWs at -0.62 V in 0.1 M $KHCO_3$, SEM image shown as inset with scale bar 5 µm. Catalysis data is shown in Supplementary Fig. 37. More SEM images are available in Supplementary Figs. 34-36.

To rule out surface area/roughness effects, we tested Cu catalysts prepared by electrodeposition (ED Cu). This process generates high surface area catalysts but does not involve an oxidized Cu intermediate

(see Methods section for details). Two catalysts were prepared; ED Cu A, which has a comparable roughness factor to OD Cu (Supplementary Table 18), and ED Cu B which has a smaller roughness factor (SEM images as insets in Figs. 4b and 4c). Fig. 4b shows that products of $^{13}CO/^{12}CO_2$ reduction -0.67 V vs RHE on ED Cu A have similar isotopic compositions. Similar results were also obtained on ED Cu B, which was tested at -0.87 V vs RHE (Fig. 4c). Since we did not observe differences in isotopic composition between the products as was the case with OD Cu, we rule out surface area/roughness as a possible explanation of our results. Additionally, it is apparent that such catalyst preparation methods do not result in creation of product specific sites.

Finally, catalyst morphology has been shown to be important in determining the selectivity of Cu catalysts.[40] To explore this effect, we synthesized an oxide-derived Cu catalyst with a distinctly different morphology from OD Cu. Oxide-derived Cu nanowire (OD Cu NWs) catalysts were synthesized according to the procedure described by Smith and co-workers[25] with some modifications (see Methods section for details and SEM images as inset in Fig. 4d). Fig. 4d shows that the isotopic compositions of ethylene, ethanol/acetate and 1-propanol obtained by reduction of $^{13}CO/^{12}CO_2$ at -0.62 V vs RHE are also different from each other. This means that like OD Cu, OD Cu NWs also possesses product specific active sites. Similarly, we can rule out the possibility that the observed differences in isotopic composition are a result of morphology effects.

Mechanistic insights. Besides the finding that the active sites on OD Cu are product specific, several other mechanistic insights can be gained from this work. To explain oxygenate generation on Cu-based catalysts from CO_2R, several research groups have proposed that mobile nonadsorbed CO can undergo an insertion reaction with surface bound $*CH_2$ species to form a $*COCH_2$ intermediate.[41–43] Further reduction of $*COCH_2$ would lead to formation of ethanol and possibly 1-propanol as well.[13] Also, Meyer and co-workers further proposed that this $*COCH_2$

intermediate could lead to the formation of acetate.[42] This type of CO insertion mechanism was first proposed by Hori and co-workers, using an analogy to Fischer-Tropsch catalysis and we will refer to it as the CO insertion mechanism.[13]

Using our approach, evidence of a CO insertion mechanism could be observed in two ways. Firstly, according to the mechanism proposed by Hori, $^{12}CO_2$ would be reduced to surface bound $*^{12}CO$ and subsequently to $*^{12}CH_2$. Labelled CO insertion would yield a $*^{13}CO^{12}CH_2$ intermediate, which then reduces to form ethanol, 1-propanol or acetate. Importantly, this mechanism predicts that the ^{13}C should be in the α carbon position (-CH_2OH) rather than the β carbon position (-CH_3). Similarly, for 1-propanol, ^{13}C would be in the α position (-CH_2OH) rather than the β (-CH_2-) or γ (-CH_3) positions. As for acetate, ^{13}C should be in the carboxyl group (-COO^-) rather than the α position (-CH_3). However, ^{13}C NMR reveals no such preference for ^{13}C to be in any of the positions relative to another (see Supplementary Figs. 39-44 for more details). Secondly, CO insertion would not produce a binomial distribution of ^{12}C and ^{13}C in the C_2 products but rather a distribution with enhanced $^{12}C^{13}C$ formation, as compared to the $^{12}C^{12}C$ or $^{13}C^{13}C$. The ^{12}C-^{13}C distributions of ethanol or acetate do not appear to display a strong bias for formation of the $^{12}C^{13}C$ product (Figs. 2 and 3, Supplementary Figs. 27 and 31). Thus, we conclude that the CO insertion mechanism does not occur in the catalyst systems in this study.

Another interesting experimental observation is that ethanol and acetate are generated from the same active sites on OD Cu. This means that these products are likely to be linked mechanistically and thus share the same selectivity determining intermediates/steps. Indeed, ethanol and acetate have been linked closely together in previous reports. Kanan and co-workers observed substantial acetate formation at high pH during CO reduction on OD Cu, which they ascribed to attack of carbonyl-containing intermediates by OH^-.[27] As the increased acetate formation at high pH was accompanied by a decrease in ethanol, it can be inferred that the products share a common intermediate. As another example, Koper and co-workers proposed that Cannizzaro disproportionation of acetaldehyde

generates both acetate and ethanol simultaneously.[44] On the other hand, our observation that ethylene and 1-propanol are generated from different sites suggest that these products do not share common selectivity determining intermediates/steps and branch early on after C-C coupling from the ethanol/acetate pathway. Additionally, our results do not support the mechanism proposed by Head-Gordon and co-workers, which places acetate on the ethylene pathway rather than on the ethanol pathway.[12]

Additionally, our experimental observations on OD Cu may also be rationalized from the point of view of scaling relations. In CO_2R, intermediates bind to the surface through the C and/or the O atom.[10,12,24,45] Because of scaling relations, intermediates that bind through the C atom are expected to have adsorption energies that are linearly related to each other, with the same rationale applying to intermediates that bind through the O atom. For ethylene selective sites, the adsorption energies of intermediates must all be shifted in a way such that after C-C coupling, formation of the ethylene intermediate is by far the most kinetically favourable compared to the ethanol/acetate or 1-propanol intermediates. On the other hand, shifting the adsorption energies of intermediates in a different way could result in favouring the formation of the ethanol/acetate intermediate or the 1-propanol intermediate. Recalling the identification of a range of strong CO adsorption sites on OD Cu not present on polycrystalline Cu by Chorkendorff and co-workers, [34] we find it possible that these strong CO adsorption sites are associated with the product specific sites that we have discovered. We further posit that these sites have specific combinations of C and O adsorption energies that enable them to become product specific. Kanan and co-workers have shown that grain boundaries are the active sites on OD Cu for the reduction of CO to C_2/C_3 products.[34,35] We therefore think it possible that the structure of each product specific active site may be a specific type of grain boundary termination.

Another consequence of scaling relations is its effect on the formation of $*^{12}CO$ from $^{12}CO_2$. Theoretical studies have predicted that the rate limiting step of this reaction is the formation of *COOH from $*CO_2$.[11,15,46]

Since we have consistently observed that ethanol/acetate have the highest ^{12}C fractions (Fig. 2a), their active sites should have the highest $^{12}CO_2$ to $*^{12}CO$ turn over frequencies. We thus posit that due to scaling relations, enhancing the formation of the $*^{12}COOH$ intermediate by tuning catalyst adsorption energies also enhances formation of the ethanol/acetate intermediate. Additionally, ethylene and 1-propanol selective sites should have different *COOH adsorption energies from ethanol/acetate selective sites since their ^{13}C fractions depend differently on the applied potential (Fig. 2a). This likely means that *COOH adsorption energies may be a descriptor for the product selectivity of an active site. Because of this, turn over frequencies for $^{12}CO_2$ and $*^{12}CO$ are active site dependent, giving each site a different probability of $*^{12}CO$ vs $*^{13}CO$. This gives rise to the different product isotopic compositions as we have observed.

Finally, a theory paper published by Goddard and co-workers could possibly offer some insight on our results and serve as a starting point towards identifying the different active sites we have observed.[47] Using molecular dynamics, they randomly generated sites on Cu nanoparticles with different atomic configurations. Approximately 9% of these generated sites had a larger CO binding energy than Cu (211). This would seem to be consistent with the temperature programmed desorption study of Chorkendorff and co-workers in which they found stronger CO binding sites on OD Cu which are not present on polycrystalline Cu.[34] Among the strong CO binding sites, the theoretical study identified 2 atomic configurations which were proposed to be active for C-C coupling. Relating these findings to our experimental work, it is conceivable that some of the sites studied by Goddard and co-workers could also be present on the OD Cu surface. It is possible that the differences in CO binding energy for different surface configuration could be used to identify C_2 and C_3 product selective sites, although more precise knowledge of the selectivity determining steps would be required.

Conclusions

In summary, we have shown via isotope labelling that OD Cu has product specific active sites for the CO_2R reaction, with one set of active sites generating ethylene, another ethanol/acetate and yet another 1-propanol. We reason that due to scaling relations, the rate of *COOH formation (intermediate to *CO) should be different on each type of active site. This means that each active site has a different probability of $*^{12}CO$ vs $*^{13}CO$ and as a result, products generated from different sites possess different isotopic compositions. In contrast, by performing similar experiments on polycrystalline Cu, Cu (100) and Cu (111) we show that these have sites that produces a mixture of C-C coupled products. Finally, our finding that active sites on OD Cu are product specific should motivate future work to understand these sites as well as ways to engineer specific types of sites into a single structure, thereby creating catalysts with very high product selectivity.

Methods

Materials. Potassium carbonate (99.995% metals basis), potassium hydroxide (99.99% metals basis), ^{13}C carbon monoxide (<5 atom % ^{18}O, 99 atom % ^{13}C), nitric acid (70%), hydrochloric acid (37%), potassium phosphate monobasic (99.99% metals basis) and potassium phosphate dibasic (99.95% metals basis) were purchased from Sigma-Aldrich. Copper foil (0.1 mm thick, 99.9999%) and glassy carbon plates were purchased from Alfa Aesar. Selemion AMV anionic exchange membranes were purchased from Asahi Glass Co., Ltd. Si wafers of various orientations were purchased from UniversityWafer, Inc. The copper sputtering target (99.999%) was purchased from Kurt J. Lesker Company. All chemicals were used without further purification. Carbon dioxide (99.995%), nitrogen (99.999%), argon (99.999%) and hydrogen (99.999%) were purchased from Praxair. Natural abundance carbon monoxide (99.999% research purity) was purchased from Matheson Tri-gas Inc. Hydrogen, argon, nitrogen and carbon dioxide gas purifiers purchased from Valco Instruments Co. Inc were used on the gas feeds to the electrochemical cell and gas chromatograph. 18.2 MΩ deionized (DI) water was produced by a Millipore system and used for electrolyte preparation.

Preparation of polycrystalline Cu (PC Cu). Cu foil was cut into 2 cm by 2 cm square pieces and then electropolished at a potential of 2V vs the counter electrode for a period of 5 minutes. The counter electrode used was another Cu foil of larger dimensions (5 cm by 5 cm).

Preparation of oxide-derived Cu (OD Cu). Oxide-derived Cu was prepared according to the procedure developed by Kanan and co-workers.[27] Cu foil was first cut into 2 cm by 2 cm square pieces and then electropolished at a potential of 2 V vs the counter electrode for a period of 5 minutes. The counter electrode used was another Cu foil of larger dimensions (5 cm by 5 cm). To oxidize the surface, the Cu foil was thermally

annealed in air using a muffle furnace at a temperature of 500 ºC for 1 hour. The muffle furnace was then allowed to cool to room temperature before removing the oxidized Cu foils.

Preparation of oriented Cu surfaces. Cu (100) and (111) oriented surfaces were prepared according to similar procedures as described by Jaramillo and co-workers.[36] Si wafers with different orientations were used as growth substrates to facilitate epitaxial growth of Cu. Cu films grown on Si (100) and (110) wafers yield Cu orientations of (100) and (111) respectively. The native oxide on the Si wafers was first removed via a HF etch and subsequent growth of the films was carried out using sputtering with an AJA International ATC Orion 5 sputtering system. In all cases, the thicknesses of the Cu films were controlled to be 200 nm thick using a quartz crystal monitor. Samples were kept in a N_2 filled glove box when not in use to minimize oxidation in ambient air. The orientations was also confirmed according to similar procedures reported by Koper and co-workers[48] as well as Yeo and co-workers.[32] Briefly, this was accomplished with cyclic voltammetry in Ar sparged 0.1 M KOH solution in the potential range of -1.3V to -0.45V vs Ag/AgCl at a rate of 120 mVs^{-1}. OH^- adsorption and desorption peaks are unique and depend on the Cu surface and thus may be used to identify and confirm its orientation. Cyclic voltammetry was also carried out after CO reduction to confirm that loss of the surface orientation did not occur. (See Supplementary Fig. 33).

Preparation of oxide-derived Cu nanowires (OD Cu NWs). Oxide-derived nanowires were prepared according to the method described by Smith and co-workers, with some modifications.[25] Firstly, Cu foil was first cut into 2 cm by 2 cm square pieces and then electropolished at a potential of 2V vs the counter electrode for a period of 5 minutes. The counter electrode used was another Cu foil of larger dimensions (5 cm by 5 cm). The Cu foil was then immersed into an aqueous solution containing 0.133 M $(NH_4)_2S_2O_8$ and 2.667 M NaOH for 10 minutes, resulting in growth of $Cu(OH)_2$ nanowires on the surface. The foil was then thermally annealed in air using a muffle furnace at a temperature of 500 °C for 30 mins to convert $Cu(OH)_2$ to CuO. The muffle furnace was then allowed to cool to room temperature before removing the Cu foils.

Preparation of electrodeposited Cu (ED Cu A and ED Cu B). ED Cu A and ED Cu B were prepared by electrodeposition of Cu onto an electropolished Cu foil using a solution containing 0.1 M $CuSO_4$ adjusted to pH 1 using concentrated H_2SO_4. A constant cathodic current density of -400 mA cm^{-2} was applied for 8 minutes for ED Cu A and only 2 minutes for ED Cu B. Such a procedure results in a dendritic, porous structure with a high surface area with the roughness factor increasing with increasing deposition time.

Materials characterization and electroactive surface area measurements. Scanning electron microscopy images were taken on a FEI Quanta 200 FEG scanning electron microscope using an accelerating voltage of 15 kV. X-ray diffraction patterns were obtained using a Rigaku Smartlab x-ray diffractometer.

Electroactive surface area measurements were performed according to procedures described by Nilsson and co-workers.[33] These measurements were performed in the same electrochemical cell as that for electrolysis experiments. 0.1 M $KHCO_3$ was used as the electrolyte and cyclic voltammetry was carried out in a region where faradaic processes do not occur. This was carried out with various scan rates and the geometric current density was plotted vs scan rate. The slope of this graph is equal to the double layer capacitance.

Electrochemical measurements. For all electrochemical measurements described in this work, a Biologic SP-300 potentiostat was used. CO reduction was carried out using a custom-made electrochemical cell made of PEEK and fitted with Teflon o-rings for chemical inertness and durability. In this cell, the working and counter electrodes are both constrained to be 1 cm^2 and sit parallel to each other in order to ensure a uniform

potential distribution across the working electrode surface. In all electrochemical CO_2/CO reduction experiments, glassy carbon was used as the counter electrode (anode) instead of Pt due to concerns regarding Pt dissolution.[49] In order to ensure that the electrolyte remains saturated with $^{12}CO_2$ and ^{13}CO throughout electrolysis, these gases were continuously introduced into the electrochemical cell at a rate of 1.5 and 3.5 sccm respectively using mass-flow controllers. A custom-made glass frit fabricated by Adams & Chittenden Scientific Glass was used to disperse the gas into the electrolyte as well as provide adequate convection in the electrochemical cell.[50] Before carrying out bulk electrolysis experiments, the gas mixture was allowed to flow through the electrolyte in the cathode chamber for at least 15 minutes to ensure that the electrolyte is saturated. To separate the electrolyte in the cathode and anode chambers, a Selemion AMV anion exchange membrane was employed. Before use, the membrane was carefully rinsed with DI water. The electrolyte volume used in both the cathode and anode were 1.8 ml each. Before use in experiments, the electrochemical cell was sonicated in 20 wt.% nitric acid for 1 hour. All bulk electrolysis experiments were conducted for 70 minutes. A leak-free Ag/AgCl electrode from Innovative Instruments, Inc was employed as a reference electrode. The accuracy of this reference electrode was ensured periodically by comparison with a custom-made reversible hydrogen electrode. To convert potentials vs Ag/AgCl to the RHE scale, the following equation as used:

$$E(vs.\,\mathrm{RHE}) = E(vs.\,\mathrm{Ag/AgCl}) + 0.197\,V + 0.0591\,pH, \quad (1)$$

After saturation of the electrolyte with the gas mixture, the solution resistance was determined using potentiostatic electrochemical impedance spectroscopy (PEIS), scanning through a frequency range of 1 MHz to 10 Hz. 85% of the solution resistance was then compensated using the software and the remaining 15% was post-corrected after the experiment.

Preparation of electrolyte and product analysis. Preparation of electrolytes and product analysis was performed according to similar procedures as reported previously.[26]

GCMS analysis of gas and liquid products. Isotopic composition of both the gas and liquid products were determined using gas chromatography-mass spectrometry (GCMS) with an Agilent 7890A GC with 5975C inert XL MSD (triple axis detector). The column used was an Agilent J&W PoraPLOT Q capillary column of length 25 m, internal diameter 0.25 mm and film thickness 8 µm (part number CP7549). Helium (99.999%) was used as the carrier gas with a flow rate of 1.0 ml/min in the column. A glass wool liner was used in the inlet, which was set to 250 °C.

For gas product analysis, 10 µl of gas was injected into the GCMS and the injection mode was split with a 1:1 ratio. For the analysis method, the selected ion monitoring (SIM) operating mode was used. Elution times of the target analytes (ethylene and ethane) were determined by injecting known standards. During the run, the operating temperature of the oven was set to 30 °C for 7.5 minutes. A bake out at 100 °C for 5 minutes was utilized at the end of each run.

For liquid product analysis, electrolyte samples were first acidified with concentrated hydrochloric acid to pH 2 to convert acetate into the acetic acid form, which is amenable to GCMS analysis. For each analysis, 0.5 µl of sample was injected and the injection mode was split with a 25:1 ratio. The selected ion monitoring (SIM) operating mode was used for liquid products. Similarly, the elution times of the target analytes (ethanol, 1-propanol and acetic acid) were determined by injecting known standards dissolved in water. During the run, the oven temperature was set to 145 °C for 10 minutes. A bake out at 200 °C for 5 minutes was utilized at the end of every run.

To ensure that the mass spectra of different products obtained with our GCMS are consistent with established databases,[51] standards of natural isotopic abundances were

also injected and all mass fragments with m/z in the range 20 to 75 were scanned (see Supplementary Figs. 11-13 for more details).

Determination of the isotopic composition based on the mass spectrometry data is explained in the Supplementary Note 4.

^{13}C NMR spectroscopy of liquid products. ^{13}C NMR was utilized to analyze the isotopic composition of the liquid products using a Bruker Avance III 500 MHz spectrometer. 700 µl of the electrolyte with the liquid products was mixed with 35 µl of D_2O containing 10 mM DMSO and 50 mM phenol. To prevent ^{1}H protons from splitting the ^{13}C nuclei, proton decoupling techniques were utilized. Samples were run for at least 12 hours to accumulate sufficient signal. Determination of the isotopic composition based on the NMR results is explained in Supplementary Note 5.

Data availability. The data that support the findings of this study are available from the corresponding author upon reasonable request.

References

1. Intergovernmental Panel on Climate Change, IPCC, Intergovernmental Panel on Climate Change & Intergovernmental Panel on Climate Change (IPCC). *Climate Change 2014: Synthesis Report*. *Contribution of Working Groups I, II and III to the Fifth Assessment Report of the Intergovernmental Panel on Climate Change* (2014).

2. Chu, S., Cui, Y. & Liu, N. The path towards sustainable energy. *Nat Mater* **16,** 16–22 (2017).

3. Hori, Y. Electrochemical CO_2 Reduction on Metal Electrodes. in *Modern Aspects of Electrochemistry SE - 3* (eds. Vayenas, C., White, R. & Gamboa-Aldeco, M.) **42,** 89–189 (Springer New York, 2008).

4. Bushuyev, O. S. *et al.* What Should We Make with CO_2 and How Can We Make It? *Joule* **2,** 825–832 (2018).

5. Raciti, D. & Wang, C. Recent Advances in CO_2 Reduction Electrocatalysis on Copper. *ACS Energy Lett.* **3,** 1545–1556 (2018).

6. Hori, Y., Murata, A. & Takahashi, R. Formation of hydrocarbons in the electrochemical reduction of carbon dioxide at a copper electrode in aqueous solution. *J. Chem. Soc. Faraday Trans. 1 Phys. Chem. Condens. Phases* **85,** 2309 (1989).

7. Kuhl, K. P., Cave, E. R., Abram, D. N. & Jaramillo, T. F. New Insights into the Electrochemical Reduction of Carbon Dioxide on Metallic Copper Surfaces. *Energy Environ. Sci.* **5,** 7050–7059 (2012).

8. Kuhl, K. P. *et al.* Electrocatalytic Conversion of Carbon Dioxide to Methane and Methanol on Transition Metal Surfaces. *J. Am. Chem. Soc.* **136,** 14107–14113 (2014).

9. Li, C. W. & Kanan, M. W. CO_2 Reduction at Low Overpotential on Cu Electrodes Resulting from the Reduction of Thick Cu_2O Films. *J. Am. Chem. Soc.* **134,** 7231–7234 (2012).

10. Peterson, A. A. *et al.* How copper catalyzes the electroreduction of carbon dioxide into hydrocarbon fuels. *Energy Environ. Sci.* **3,** 1311–1315 (2010).

11. Cheng, T., Xiao, H. & Goddard, W. A. Reaction Mechanisms for the Electrochemical Reduction of CO_2 to CO and Formate on the Cu(100) Surface at 298 K from Quantum Mechanics Free Energy Calculations with Explicit Water. *J. Am. Chem. Soc.* **138,** 13802–13805 (2016).

12. Garza, A. J., Bell, A. T. & Head-Gordon, M. Mechanism of CO_2 Reduction at Copper Surfaces: Pathways to C_2 Products. *ACS Catal.* **8,** 1490–1499 (2018).

13. Hori, Y., Takahashi, R., Yoshinami, Y. & Murata, A. Electrochemical Reduction of CO at a Copper Electrode. *J. Phys. Chem. B* **101,** 7075–7081 (1997).

14. Schouten, K. J. P., Qin, Z., Gallent, E. P. & Koper, M. T. M. Two Pathways for the Formation of Ethylene in CO Reduction on Single-Crystal Copper Electrodes. *J. Am. Chem. Soc.* **134,** 9864–9867 (2012).

15. Kortlever, R., Shen, J., Schouten, K. J. P., Calle-Vallejo, F. & Koper, M. T. M. Catalysts and Reaction Pathways for the Electrochemical Reduction of Carbon Dioxide. *J. Phys. Chem. Lett.* **6,** 4073–4082 (2015).

16. Calle-Vallejo, F. & Koper, M. T. M. Theoretical Considerations on the Electroreduction of CO to C_2 Species on Cu(100) Electrodes. *Angew. Chemie* **125,** 7423–7426 (2013).

17. Dinh, C. T. *et al.* CO_2 electroreduction to ethylene via hydroxide-mediated copper catalysis at an abrupt interface. *Science* **360,** 783–787 (2018).

18. Ma, S. *et al.* One-step electrosynthesis of ethylene and ethanol from CO_2 in an alkaline electrolyzer. *J. Power Sources* **301,** 219–228 (2016).

19. Peterson, A. A. & Nørskov, J. K. Activity Descriptors for CO_2 Electroreduction to Methane on Transition-Metal Catalysts. *J. Phys. Chem. Lett.* **3,** 251–258 (2012).

20. Hansen, H. A., Varley, J. B., Peterson, A. A. & Nørskov, J. K. Understanding Trends in the Electrocatalytic Activity of Metals and Enzymes for CO_2 Reduction to CO. *J. Phys. Chem. Lett.* **4,** 388–392 (2013).

21. Liu, X. *et al.* Understanding trends in electrochemical carbon dioxide reduction rates. *Nat. Commun.* **8,** (2017).

22. Sandberg, R. B., Montoya, J. H., Chan, K. & Nørskov, J. K. CO-CO coupling on Cu facets: Coverage, strain and field effects. *Surf. Sci.* **654,** 56–62 (2016).

23. Goodpaster, J. D., Bell, A. T. & Head-Gordon, M. Identification of Possible Pathways for C–C Bond Formation during Electrochemical Reduction of CO_2: New Theoretical Insights from an Improved Electrochemical Model. *J. Phys. Chem. Lett.* **7,** 1471–1477 (2016).

24. Cheng, T., Xiao, H. & Goddard, W. A. Full atomistic reaction mechanism with kinetics for CO reduction on Cu(100) from ab initio molecular dynamics free-energy calculations at 298 K. *Proc. Natl. Acad. Sci.* **114,** 1795–1800 (2017).

25. Ma, M., Djanashvili, K. & Smith, W. A. Controllable Hydrocarbon Formation from the Electrochemical Reduction of CO_2 over Cu Nanowire Arrays. *Angew. Chemie Int. Ed.* **55,** 6680–6684 (2016).

26. Lum, Y., Yue, B., Lobaccaro, P., Bell, A. T. & Ager, J. W. Optimizing C-C Coupling on Oxide-Derived Copper Catalysts for Electrochemical CO_2 Reduction. *J. Phys. Chem. C* **121,** 14191–14203 (2017).

27. Li, C. W., Ciston, J. & Kanan, M. W. Electroreduction of carbon monoxide to liquid fuel on oxide-derived nanocrystalline copper. *Nature* **508,** 504–507 (2014).

28. Ren, D. *et al.* Selective Electrochemical Reduction of Carbon Dioxide to Ethylene and Ethanol on Copper(I) Oxide Catalysts. *ACS Catal.* **5,** 2814–2821 (2015).

29. Kas, R., Kortlever, R., Yılmaz, H., Koper, M. T. M. & Mul, G. Manipulating the Hydrocarbon Selectivity of Copper Nanoparticles in CO_2 Electroreduction by Process Conditions. *ChemElectroChem* **2,** 354–358 (2014).

30. Raciti, D. *et al.* Low-Overpotential Electroreduction of Carbon Monoxide Using Copper Nanowires. *ACS Catal.* **7,** 4467–4472 (2017).

31. Mistry, H. *et al.* Highly selective plasma-activated copper catalysts for carbon dioxide reduction to ethylene. *Nat. Commun.* **7,** 12123 (2016).

32. Huang, Y., Handoko, A. D., Hirunsit, P. & Yeo, B. S. Electrochemical Reduction of CO_2 Using Copper Single-Crystal Surfaces: Effects of CO* Coverage on the Selective Formation of Ethylene. *ACS Catal.* **7,** 1749–1756 (2017).

33. Roberts, F. S., Kuhl, K. P. & Nilsson, A. High Selectivity for Ethylene from Carbon Dioxide Reduction over Copper Nanocube Electrocatalysts. *Angew. Chemie* **127,** 5268–5271 (2015).

34. Verdaguer-Casadevall, A. *et al.* Probing the Active Surface Sites for CO Reduction on Oxide-Derived Copper Electrocatalysts. *J. Am. Chem. Soc.* **137,** 9808–9811 (2015).

35. Feng, X., Jiang, K., Fan, S. & Kanan, M. W. A Direct Grain-Boundary-Activity Correlation for CO Electroreduction on Cu Nanoparticles. *ACS Cent. Sci.* **2,** 169–174 (2016).

36. Hahn, C. *et al.* Engineering Cu surfaces for the electrocatalytic conversion of CO_2: Controlling selectivity toward oxygenates and hydrocarbons. *Proc. Natl. Acad. Sci.* **114,** 5918–5923 (2017).

37. Singh, M. R., Clark, E. L. & Bell, A. T. Effects of electrolyte, catalyst, and membrane composition and operating conditions on the performance of solar-driven electrochemical reduction of carbon dioxide. *Phys. Chem. Chem. Phys.* **17,** 18924–36 (2015).

38. Xiao, H., Cheng, T., Goddard, W. A. & Sundararaman, R. Mechanistic Explanation of the pH Dependence and Onset Potentials for Hydrocarbon Products from Electrochemical Reduction of CO on Cu (111). *J. Am. Chem. Soc.* **138,** 483–486 (2016).

39. Resasco, J., Lum, Y., Clark, E., Zeledon, J. Z. & Bell, A. T. Effects of Anion Identity and Concentration on Electrochemical Reduction of CO_2. *ChemElectroChem* **5,** 1064–1072 (2018).

40. Dutta, A., Rahaman, M., Luedi, N. C., Mohos, M. & Broekmann, P. Morphology Matters: Tuning the Product Distribution of CO_2 Electroreduction on Oxide-Derived Cu Foam Catalysts. *ACS Catal.* **6,** 3804–3814 (2016).

41. Lee, S., Park, G. & Lee, J. Importance of Ag–Cu Biphasic Boundaries for Selective Electrochemical Reduction of CO_2 to Ethanol. *ACS Catal.* **7,** 8594–8604 (2017).

42. Wang, Y. *et al.* CO_2 reduction to acetate in mixtures of ultrasmall $(Cu)_n$,$(Ag)_m$ bimetallic nanoparticles. *Proc. Natl. Acad. Sci.* **115,** 278–283 (2018).

43. Ren, D., Ang, B. S.-H. & Yeo, B. S. Tuning the Selectivity of Carbon Dioxide Electroreduction toward Ethanol on Oxide-Derived Cu_xZn Catalysts. *ACS Catal.* **6,** 8239–8247 (2016).

44. Birdja, Y. Y. & Koper, M. T. M. The Importance of Cannizzaro-Type Reactions during Electrocatalytic Reduction of Carbon Dioxide. *J. Am. Chem. Soc.* **139,** 2030–2034 (2017).

45. Calle-Vallejo, F. & Koper, M. T. M. Theoretical Considerations on the Electroreduction of CO to C_2 Species on Cu(100) Electrodes. *Angew. Chemie Int. Ed.* **52,** 7282–7285 (2013).

46. Singh, M. R., Goodpaster, J. D., Weber, A. Z., Head-Gordon, M. & Bell, A. T. Mechanistic insights into electrochemical reduction of CO_2 over Ag using density functional theory and transport models. *Proc. Natl. Acad. Sci. U. S. A.* **114,** E8812–E8821 (2017).

47. Cheng, T., Xiao, H. & Goddard, W. A. Nature of the Active Sites for CO Reduction on Copper Nanoparticles; Suggestions for Optimizing Performance. *J. Am. Chem. Soc.* **139,** 11642–11645 (2017).

48. Pérez-Gallent, E., Marcandalli, G., Figueiredo, M. C., Calle-Vallejo, F. & Koper, M. T. M. Structure- and Potential-Dependent Cation Effects on CO Reduction at Copper Single-Crystal Electrodes. *J. Am. Chem. Soc.* **139,** 16412–16419 (2017).

49. Chen, J. G., Jones, C. W., Linic, S. & Stamenkovic, V. R. Best Practices in Pursuit of Topics in Heterogeneous Electrocatalysis. *ACS Catal.* **7,** 6392–6393 (2017).

50. Lobaccaro, P. *et al.* Effects of temperature and gas–liquid mass transfer on the operation of small electrochemical cells for the quantitative evaluation of CO_2 reduction electrocatalysts. *Phys. Chem. Chem. Phys.* **18,** 26777–26785 (2016).

51. NIST Mass Spec Data Center, S.E. Stein, director, 'Mass Spectra' in NIST Chemistry WebBook, NIST Standard Reference Database Number 69, Eds. P.J. Linstrom and W.G. Mallard, National Institute of Standards and Technology, Gaithersburg MD, 20899.

Acknowledgements

This material is based upon work performed by the Joint Center for Artificial Photosynthesis, a DOE Energy Innovation Hub, supported through the Office of Science of the U.S. Department of Energy under Award Number DE-SC0004993. Y.L. acknowledges the support of an A*STAR National Science Scholarship. We thank Aya Buckley for assistance with ^{13}C NMR spectroscopy and Wan Ru Leow for assistance with the creation of figures.

Author contributions

Y.L and J.WA. conceived and designed the experiments. Y.L conducted all the experimental work and analysed the data. All authors discussed the results and wrote the manuscript.

Competing interests

The authors declare no competing interests.